Acta Geochim (2022) 41(6):911–925
https://doi.org/10.1007/s11631-022-00567-6

ORIGINAL ARTICLE

Fractionation mechanism of iron isotopes in highly fractionated granites from the Xinxian Pluton, Western Dabie Orogen, Central China

Chenglai Deng[1,2] · **Changqing Hu**[1] · **Qiuyu Wen**[3] · **Wenbin Yang**[1] · **Wu Li**[1]

Received: 15 May 2022 / Revised: 15 August 2022 / Accepted: 15 August 2022 / Published online: 5 October 2022

Abstract Iron isotopes are important for tracing the magmatic process. The fractionation of iron isotopes in granite is up to 0.55 ‰. In this study, Wangjiagou (XWJ) granite and Tayueping (XTY) granite in the Xinxian pluton of the Western Dabie orogen were evaluated. Both the XTY and XWJ granite belong to monzogranites, with high SiO_2 (74.42–76.82 wt.%) contents. The granites are depleted of Nb and Ti but enriched with Pb and K, and they display negative Eu anomalies (Eu/Eu* = 0.40–0.52) on REE plots that are normalized by chondrite. The δ^{56}Fe values of the XTY granites vary from 0.19 ± 0.03 ‰ to 0.27 ± 0.04‰, and the δ^{56}Fe values of the XWJ granites are 0.34 ± 0.02 ‰ and 0.36 ± 0.01 ‰, respectively. Both the XTY and the XWJ granites belong to highly fractionated granites due to their SI (solidification index), DI (differentiation index), and content of CaO. Evidence from the iron isotopes shows that neither fluid exsolution, alteration, weathering, nor partial melting can explain the enrichment of the heavy iron isotopes. The results modeled using the Rayleigh equation showed that fractional crystallization can produce $\Delta^{56}Fe_{melt\text{-}crystal}$ with the value of 0.08–0.15 ‰. In conclusion, fractional crystallization was the main factor controlling the fractionation of iron isotopes, and the change of melt composition may also lead to the enrichment of heavy iron isotopes in the residual melt.

Keywords Iron isotope · Fractionated granite · Dabie orogen · Fractionation mechanism

✉ Wu Li
liwu@cumt.edu.cn

[1] Key Laboratory of Coalbed Methane Resource and Reservoir Formation Process, Ministry of Education, China University of Mining and Technology, Xuzhou 221116, People's Republic of China

[2] School of Earth Resources, China University of Geosciences, Wuhan 430074, China

[3] Metal Stable Isotope Geochemistry Laboratory, University of Science and Technology of China, Hefei 230026, China

1 Introduction

Iron has four isotopes (^{54}Fe, ^{56}Fe, ^{57}Fe, and ^{58}Fe) and three common valence states (0, + 2, + 3). Significant fractionation of iron isotopes occurred during the magmatic process in the range of −0.03‰ to 0.55‰ (Zhu et al. 2016; Du et al. 2017). Xu et al. (2017) reported that seven migmatites produced $\Delta^{56}Fe_{leucosome\text{-}melanosome}$ of about 0.09 ± 0.06 ‰, which showed that the partial melting of crustal rocks promoted the enrichment of heavy iron isotopes in melts. Wu et al. (2017a, b) argued that the high δ^{56}Fe values of most high-silica granitic rocks may not be caused by the accumulation of feldspar, by investigating the δ^{56}Fe values of the main diagenetic minerals (e.g., plagioclase, K-feldspar, and biotite) in high-silica granites, and leucosomes derived from the different source rock. Recently, Du et al. (2019) analyzed three different types of high-silica granites and suggested that the crystallization of iron–titanium oxide minerals containing ferrous ions was the main reason for the high δ^{56}Fe values in granite. Generally, previous studies have proposed four possible mechanisms that govern iron isotopic fractionation: (1) partial melting (Williams et al. 2005; Weyer and Ionov 2007; Telus et al. 2012; Xu et al. 2017); (2) fractional crystallization (Schuessler et al. 2009; Teng et al. 2011; Sossi et al. 2012; Collinet et al. 2017; Du et al. 2019; Chen et al. 2021; Deng et al. 2021; Liang et al. 2022); (3) exsolved fluids (Poitrasson and Freydier 2005; Heimann et al. 2008; Du et al. 2019; Deng et al. 2022); and (4) alteration and weathering (Poitrasson et al. 2008; Liu et al. 2014).

Highly fractionated granites (HFG) have usually undergone a high degree of "crystal-melt differentiation" processing such as fractional crystallization, which may have led to the fractionation of iron isotopes. Wu et al. (2017a, b) argued that The presence of characteristic accessory minerals such as tourmaline and lepidolite indicates that the sample is highly fractionated granite (Wu et al. 2017a, b). After integrating a large amount of granite data, it was found that the above characteristic accessory minerals were not universal (Yang 2019), however, they demonstrated a common feature of having dark minerals constituting less than 10% of the whole. The controlling fractional mechanism of iron isotopes in highly fractionated granites remains an open question. The iron isotopic composition of seven highly fractionated granites from the Western Dabie orogen is presented in this study, to discover the controlling fractional mechanism of iron isotopes in highly fractionated granites.

2 Geological background and samples

The Dabie orogen is usually divided into two areas by the Shangcheng–Macheng fault from east to west, namely the Eastern Dabie orogen and the Western Dabie orogen, respectively (Fig. 1). The Western Dabie orogen was located in the west segment of the whole Dabie orogen, and was extremely active in magmatism during the Mesozoic era as a result of the northern frontier of the Yangtze Block (YB) subducts into the North China Block (NCB) (Li et al. 1999; Zheng et al. 2003a; Zhao et al. 2007; Suo et al. 2012; Xu et al. 2012; Liu et al. 2014; Niu and Freydier 2020). The geological activities between NCB and YB changed from collision and compression into extension until the Early Cretaceous ($\sim$ 130 Ma), thus resulting in the collapse of thickened crust and the ascent of mantle material (Xu et al. 2007; Zheng 2008; He et al. 2011, 2013; Chen et al. 2013b, a; Zhu et al. 2019).

As reported in many studies, numerous high-silica granite plutons were exposed in the study area (Fig. 1) (Meng 2013; Chen et al. 2013b,2015; Huang et al. 2018). Reported Sr–Nd isotope data has indicated that the Xinxian pluton was derived from the lower crust of the northern margin of the YB without assimilation or contamination (Chen et al. 2013a; Yang et al. 2020). In terms of the identification of source rock and the age of the Xinxian pluton, previous studies on Sr–Nd–Pb–Hf isotopes have been carried out in detail (Chen et al. 2013a, 2020; Zhou et al. 2013). It is believed that the Xinxiang pluton was formed by the partial melting of TTG type magmatic rocks with a crustal depth of less than 35 km, and the zircon U–Pb age ranges from 134.3 ± 1.4 to 125.5 ± 1.5 Ma, which indicates that they were formed during the tectonic mechanism transition of the Dabie orogenic belt. Zhao et al. (2013) reported that the diagenetic temperature of the Xinxian pluton may be lower than 759 °C, the pressure may be at 1.15–2.07 kbar, and the corresponding depth may be 4.3–7.6 km, by calculation with a mineral thermobarometer.

3 Analytical methods

The whole-rock major element compositions were analyzed by X-ray fluorescence spectrometry (XRF) and the whole-rock trace elements were determined by Inductively Coupled Plasma Mass Spectrometer (ICP-MS) at the ALS Chemex (Guangzhou) Co., Ltd. The relative standard deviation (RSD) for the major elements was 3%–5%, and it was 10% lower for trace elements. The sample was decomposed with HF-H_2SO_4, the remaining F in the solution was added to H_3BO_3 for complexation, the content of ferrous (Fe^{2+}) was titrated with reference $K_2Cr_2O_7$ with sodium diphenylamine sulfonate as an indicator, and the amount of FeO was calculated. The content of ferric iron was calculated based on the measured total iron and ferrous iron content.

Fe isotope compositions were measured in the Metal Stable Isotopes Geochemistry Laboratory at the University of Science and Technology of China (USTC), Hefei, China. The digestion and evaporation procedures were carried out as described by Xia et al. (2017). The purification procedures for the iron isotopes were described by Huang et al. (2011). The sample solution was performed on the Neptune-Plus MC-ICP-MS and analyzed with the sample-standard bracketing (SSB) method. The analytical procedures for Fe isotopes were as described by Xia et al. (2017). Each sample was typically measured three times. Isotopic data were reported using the delta (δ) notation and expressed as

$$\delta^{i}\mathrm{Fe} = \left[\left({}^{i}\mathrm{Fe}/{}^{54}\mathrm{Fe}\right)_{\mathrm{sample}} / \left({}^{i}\mathrm{Fe}/{}^{54}\mathrm{Fe}\right)_{\mathrm{standard}} - 1\right] \times 1000(‰) \quad (1)$$

where i refers to mass 56 or 57.

The international standards BIR-1 and RGM-1 were purified and measured together with unknown samples, yielding δ^{56}Fe values of 0.05 ± 0.01 ‰ (n = 3, 2SD) and 0.19 ± 0.02 ‰ (n = 3, 2SD). The measured standard values agree with previously published data within error for both Fe isotopes (Xia et al. 2017).

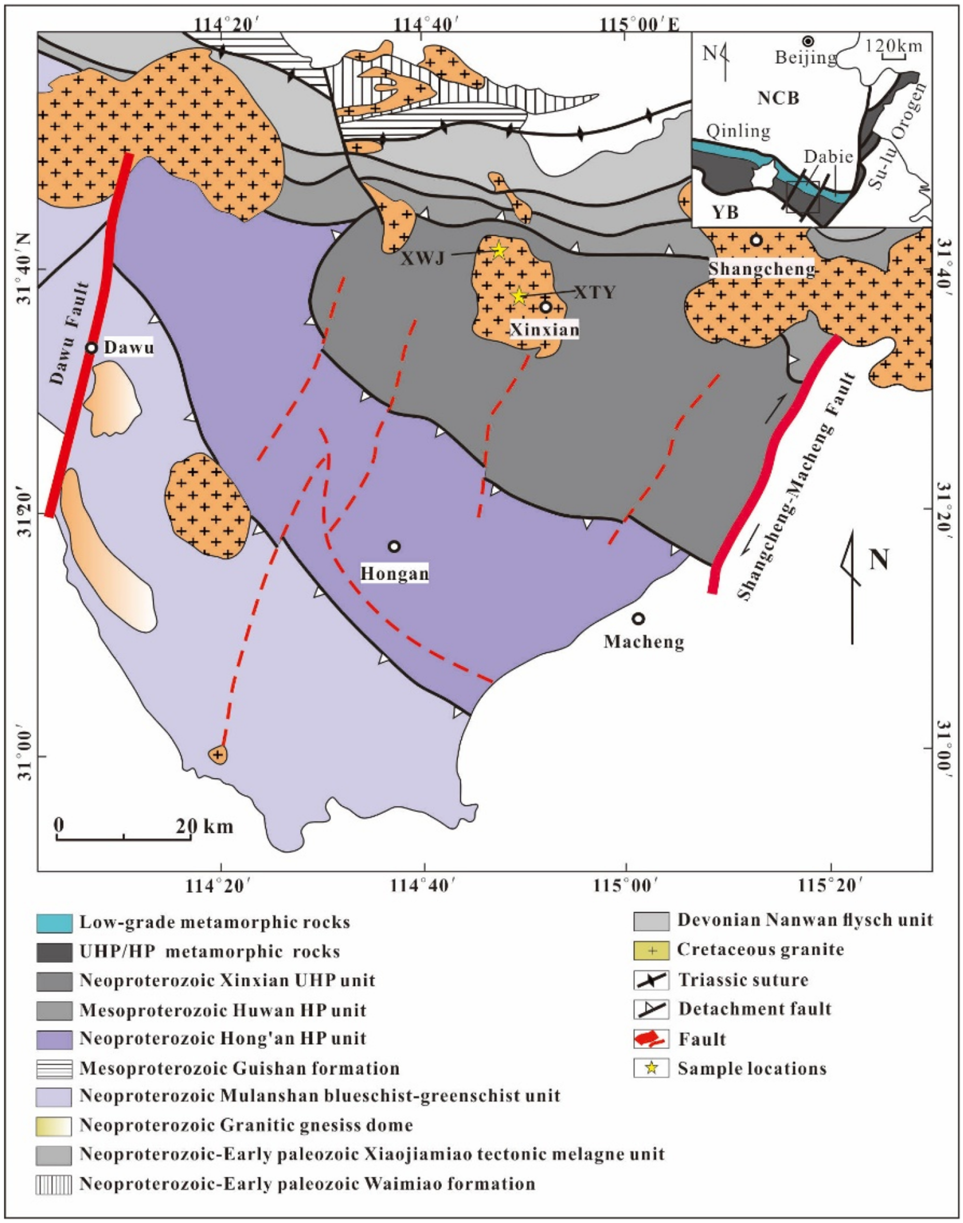

Fig. 1 Geological sketch map of Western Dabie area (modified after Zheng et al. 2003b; Liu et al. 2004)

4 Results

4.1 Major elements of samples

The analytical results of the major element composition of the samples are given in Table 1. All seven samples contained high SiO_2 (74.42–76.82 wt.%, average: 75.53 wt.%), K_2O (4.40–4.81 wt.%, average: 4.64 wt.%), and Na_2O (3.76–4.25 wt.%, average: 4.01 wt.%); and low MgO (0.07–0.29 wt.%, average: 0.17 wt.%). It has previously been established that the content of $Fe_2O_3^T$ in XTY granite (average: 1.16 wt.%) was twice that of the content of $Fe_2O_3^T$ in XWJ granite (average: 0.54 wt.%).

4.2 Trace elements of samples

The analytical results of the trace element composition of the samples are listed in Table 1. The total REE concentration of the seven granitic samples ranged from 74 to 223 ppm and enriched in LREE with the values of $(La/Yb)_N$ ranging from 10.33 to 15.71, which demonstrated that negative Eu anomalies (Eu/Eu* = 0.40–0.52) on the REE plots were normalized by chondrite (Fig. 2a). They were characterized by being enriched in Pb, K, U, and Th, and lacking Nb, Ti, Sr, and Ba, as shown in the trace element spider diagram that was normalized by a primitive-mantle (Fig. 2b).

Table 1 Major (wt.%) and trace elemental (ppm) compositions of granites from Xinxian pluton

Composition	The XTY granite					The XWJ granite	
	XTY-1-001	XTY-2-001	XTY-3-002	XTY-3-003	XTY-4-002	XWJ-001	XWJ-003
SiO_2	75.75	75.05	75.68	74.42	74.84	76.11	76.82
Al_2O_3	13.14	13.25	12.99	13.40	13.42	13.34	12.81
BaO	0.04	0.06	0.06	0.07	0.07	0.02	0.03
CaO	0.43	0.65	0.84	1.14	0.86	0.45	0.43
$Fe_2O_3^T$	0.88	1.14	1.12	1.35	1.33	0.55	0.53
K_2O	4.73	4.81	4.65	4.40	4.80	4.53	4.45
MgO	0.13	0.18	0.17	0.29	0.27	0.07	0.09
MnO	0.04	0.05	0.05	0.05	0.06	0.05	0.02
Na_2O	4.11	3.76	3.86	4.07	3.89	4.13	4.25
P_2O_5	0.01	0.02	0.03	0.05	0.04	< 0.01	0.01
TiO_2	0.11	0.15	0.15	0.19	0.18	0.06	0.07
FeO	0.29	0.32	0.38	0.54	0.45	0.06	0.07
Fe^{3+}	0.39	0.55	0.49	0.52	0.58	0.34	0.32
$Fe^{3+}/\sum Fe$	0.44	0.48	0.43	0.38	0.43	0.61	0.60
SI	0.01	0.02	0.02	0.03	0.03	0.01	0.01
LOI	0.35	0.45	0.44	0.67	0.65	0.53	0.35
Ce	58.80	76.70	81.90	94.50	98.50	24.50	28.10
Dy	1.84	2.26	2.43	2.98	2.97	0.84	0.89
Er	1.14	1.32	1.36	1.71	1.76	0.57	0.68
Eu	0.42	0.55	0.59	0.72	0.67	0.16	0.16
Ga	17.40	20.80	19.15	20.50	20.80	22.90	21.50
Gd	1.99	2.71	2.76	3.60	3.42	0.80	1.00
Ge	0.24	0.38	0.42	0.46	0.51	0.33	0.33
Hf	4.30	4.80	4.20	5.40	5.20	2.70	3.50
Ho	0.38	0.45	0.49	0.61	0.60	0.18	0.21
La	32.20	36.20	45.00	49.20	55.70	12.90	14.40
Lu	0.26	0.29	0.26	0.32	0.35	0.17	0.19
Nb	19.40	28.00	18.50	20.00	23.80	28.10	28.00
Nd	19.10	24.50	26.10	32.20	33.30	7.50	8.40
Pb	28.70	29.50	30.60	28.40	29.30	38.00	34.80
Pr	6.12	7.50	8.38	9.93	10.65	2.57	2.86
Rb	192	244	237	220	244	352	320
Sm	2.74	3.90	3.97	4.96	4.96	1.15	1.34
Sr	81.30	132.00	155.00	193.00	171.50	46.80	57.90
Ta	2.10	2.40	1.40	1.50	1.90	2.70	2.30
Th	24.30	37.50	30.20	41.30	44.30	22.00	21.10
Tm	0.19	0.22	0.21	0.27	0.29	0.11	0.13
U	4.40	10.30	3.71	3.51	6.31	7.83	5.16
Yb	1.47	1.63	1.53	1.90	2.06	0.90	1.00
Zr	130	144	148	186	178	54	71
$\sum REE$	142.40	176.70	191.80	220.30	233.10	74.60	80.00
$(La/Yb)_N$	15.71	15.93	21.13	18.57	19.39	10.28	10.33
Eu/Eu*	0.52	0.49	0.52	0.50	0.47	0.48	0.40
$10^4 \times Ga/Al$	2.51	2.96	2.78	2.88	2.92	3.21	3.17

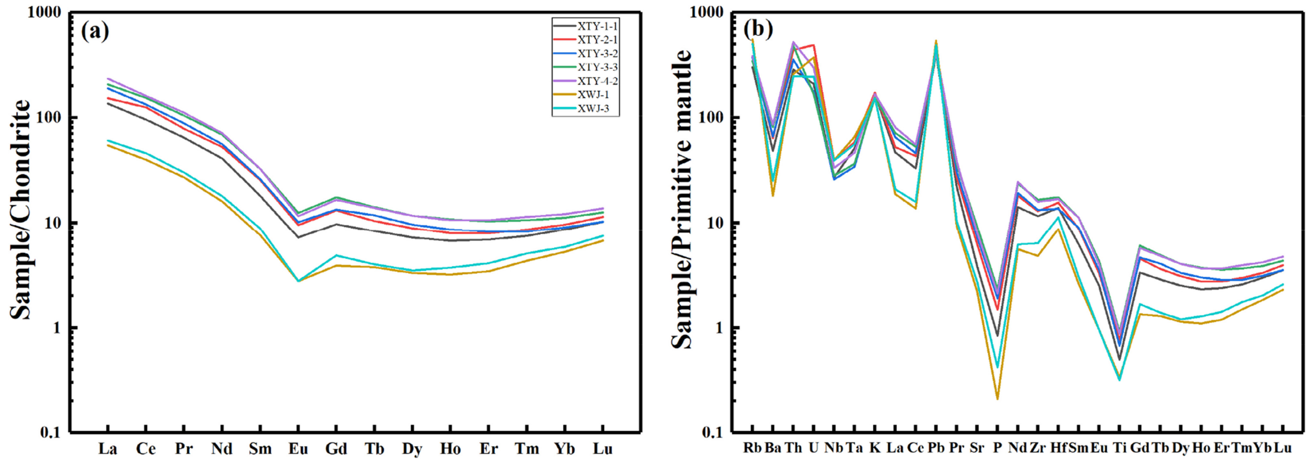

Fig. 2 Plots of chondrite-normalized REE (**a**) and primitive mantle-normalized trace elements (**b**) of the Xinxian pluton. Chondrite and primitive mantle-normalized values are from McDonough and Sun (1995) and Sun and McDonough (1989)

4.3 Fe isotopes of samples

Fe isotope data are presented in Table 2. The δ^{56}Fe values for all the samples in this study ranged from 0.19 to 0.36‰. The XWJ granite had the highest δ^{56}Fe values (0.36 ± 0.01‰, 2SD, n = 3). However, with the δ^{56}Fe values ranging from 0.19 ± 0.03‰ to 0.27 ± 0.04‰, the composition of Fe isotopes in the XTY granite was slightly less than those in the XWJ granite.

Table 2 Iron isotopes composition of HFG from Xinxian pluton and NG from eastern Dabie. Superscript * denote data from He et al. 2017

Sample	Rock type	δ^{56}Fe(‰)	2SD	δ^{57}Fe(‰)	2SD	n
XTY-1-001	HFG	0.27	0.02	0.4	0.06	3
XTY-2-001		0.2	0.05	0.29	0.1	3
XTY-3-002		0.22	0.02	0.34	0.14	3
XTY-3-003		0.27	0.04	0.34	0.05	3
XTY-4-002		0.19	0.03	0.33	0.05	3
XWJ-001		0.34	0.02	0.49	0.06	3
XWJ-003		0.36	0.01	0.63	0.05	3
06FS-1*	NG	0.061	0.051	0.102	0.072	9
06FS-4*		0.122	0.051	0.178	0.072	9
06ZY-2*		0.099	0.029	0.128	0.042	9
07YC-1*		0.139	0.023	0.229	0.04	9
07YC-3*		0.153	0.023	0.24	0.04	9
07XM-3*		0.143	0.023	0.211	0.04	9
BIR-1	Basalt	0.05	0.01	0.07	0.07	3
RGM-1	Rhyolite	0.19	0.02	0.28	0.06	3

5 Discussion

5.1 Petrogenesis of highly fractionated granites

Seven samples were collected from two sites in the Xinxian pluton; five samples were obtained near the Xinxian county; the other two were obtained from the south of the Wangjiagou reservoir. They are referred to as XTY granite and XWJ granite, respectively, hereafter. The XTY granite (Fig. 3) consisted of plagioclase (30%–35%), K-feldspar (~ 35%), quartz (20%–25%), and biotite (~ 5%). The composition of XWJ granite was similar to the XTY granite, but the content of biotite in XWJ granite was less than 5%, which was less than the biotite content in XTY granite. Both were monzogranite.

Granites can be classified into four types, namely I, S, M, and A (Chappel and White 1992; Loiselle and Wones 1979). Chen et al. (2013a) discovered that the Xinxian pluton comprises I-type granite, and its classification has been described in detail and is not repeated in this study. However, the degree of fractionation can be further interpreted, to provide more constraints from the perspective of mineralogy and major elements in this study.

The main dark mineral in the seven samples was biotite with the absence of hornblende, and its content ranged from 3 to 10% (Fig. 10a). The $10^4 \times$ Ga/Al ratios were out of the range of A-type granite ($10^4 \times$ Ga/Al = 2.6, Whalen et al. 1987) which varied from 2.51 to 3.20 in this study. Previous studies (Cin-ty and Douglas 2015; Yang 2019) revealed that the major elemental content in highly fractionated granite was CaO < 1 wt.%, SiO_2 > 72 wt.%, and

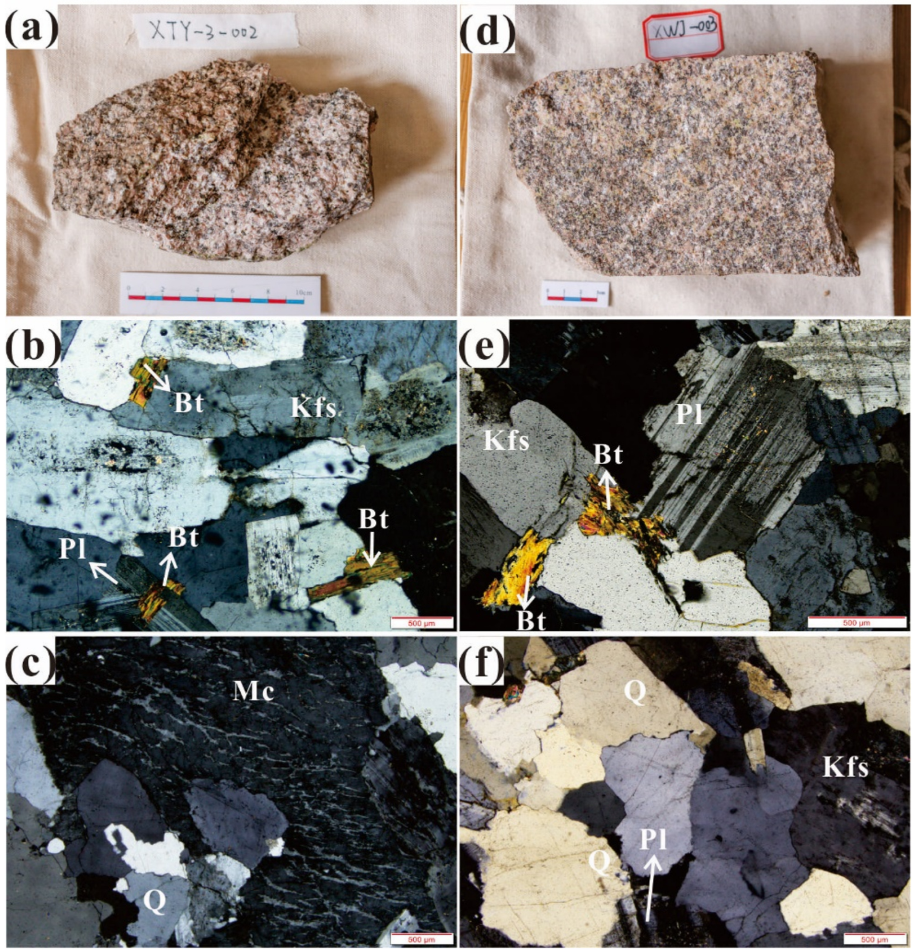

Fig. 3 Specimen photographs and photomicrographs of the Xinxian pluton. **a** The specimen photographs of the XTY granite. **b** and **c** are the minerals in the XTY granite, **d** is the specimen photographs of the XWJ granite, and **e** and **f** are the polysynthetic twin of plagioclase and biotite in the XWJ granite. Pl, plagioclase; Kfs, K-feldspar; Q, quartz; Bt, Biotite; Mc, Microline

$Na_2O + K_2O > 7$ wt.%. Meanwhile, its SI [solidification index, $MgO/(MgO + Fe_2O_3 + Na_2O + K_2O)$] should be less than 6, and the DI (differentiation index, Q + Or + Ab + Ne + Lc + Kp, all six minerals were calculated by CIPW, the results are listed in Table 3) should be more than 88. According to Table 1, the CaO contents of the seven samples were all less than 1 wt.%. The SI ranged from 0.007 to 0.029, by calculation. According to the results of the CIPW calculation (Table 3), the contents of Q, Or, and Ab were more than 88, not including the whole content of the DI. As shown in Fig. 4c, and d, the samples in our study were all plotted within the FG area. In summary, it was confirmed that the samples belong to highly differentiated I-type granite.

In this study, the U–Pb ages, as measured by a previous study, were collected (Fig. 5). As shown in Fig. 5, the diagenetic age of the Xinxian pluton is between 153.4 ± 1.1 and 125.5 ± 1.5 Ma, and the corresponding geological background is from the tectonic transformative stage of the YB (Yangtze Block) and NCB (North China Block), with the two blocks turning from the collision to the extension. In Fig. 6, the samples from the Xinxian pluton were obtained from the syn-collisional granite area. Combined with the geological background, this indicates

Table 3 Selected calculation results of CIPW standard minerals

	XTY-1-001	XTY-2-001	XTY-3-002	XTY-3-003	XTY-4-002	XWJ-001	XWJ-003
Q	32.89	33.57	33.63	31.31	31.83	33.99	34.26
Or	28.20	28.77	27.67	26.24	28.53	27.00	26.47
Ab	35.08	32.20	32.89	34.76	33.11	35.24	36.19
An	2.08	3.13	4.00	5.35	4.03	2.18	2.08
Mt	0.57	0.77	0.71	0.76	0.84	0.18	0.08
Il	0.21	0.28	0.28	0.36	0.34	0.11	0.1
Ap	0.02	0.04	0.07	0.11	0.09	0.02	0.02

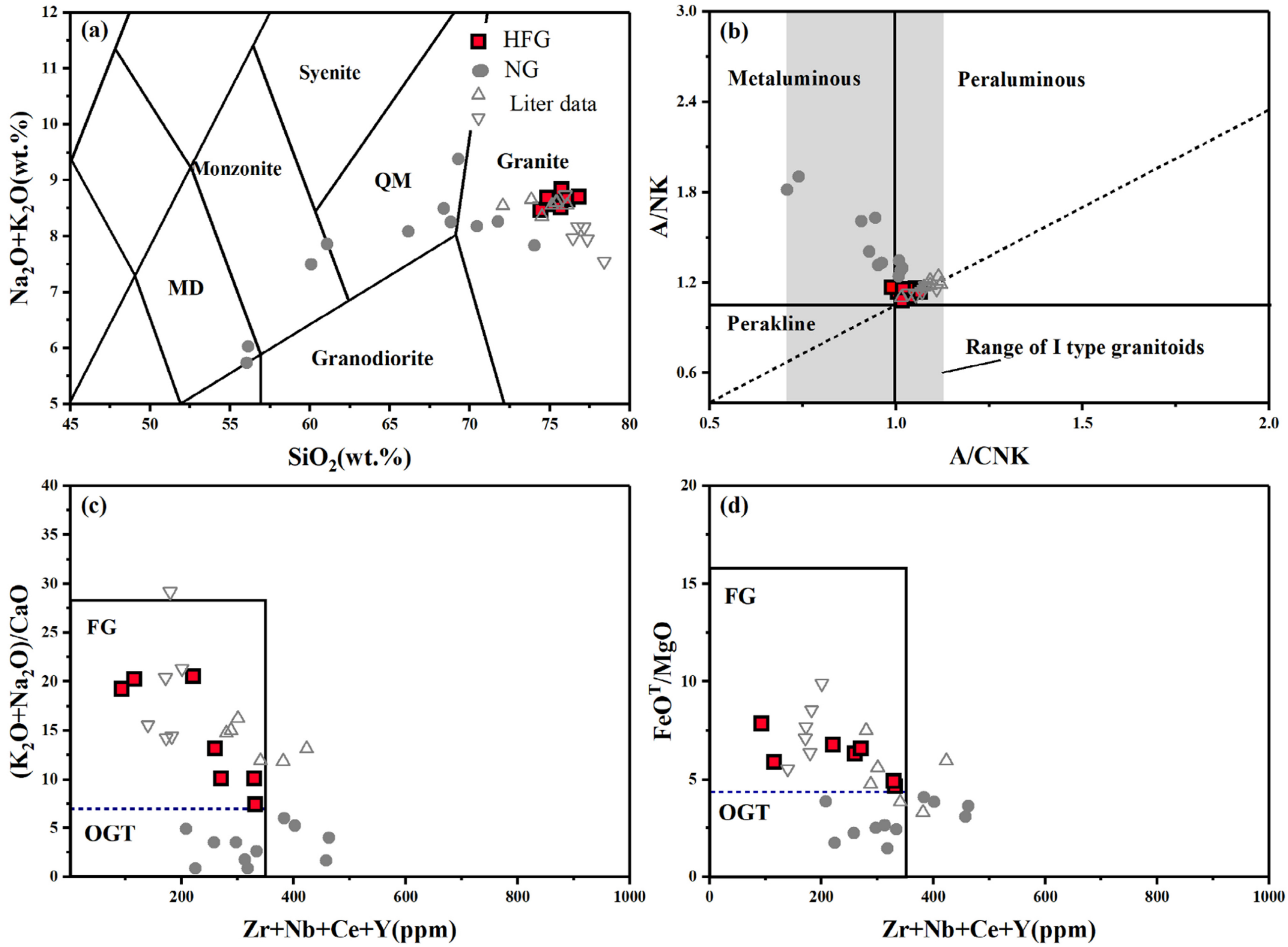

Fig. 4 Total alkali versus SiO_2 (Middlemost 1985) where MD and QM stand for mozodiorite and quartz monzonite, ANK versus ACNK, and the discrimination diagrams of (FeOt + MgO) versus (Zr + Nb + Ce + Y), in which, $x = 350$, $y = 4$ and 16 (c) and ($Na_2O + K_2O$)/CaO versus (Zr + Nb + Ce + Y), the x = 350, y = 7 and 28 (d) for the XTY and XWJ granite (after Whalen et al 1987)

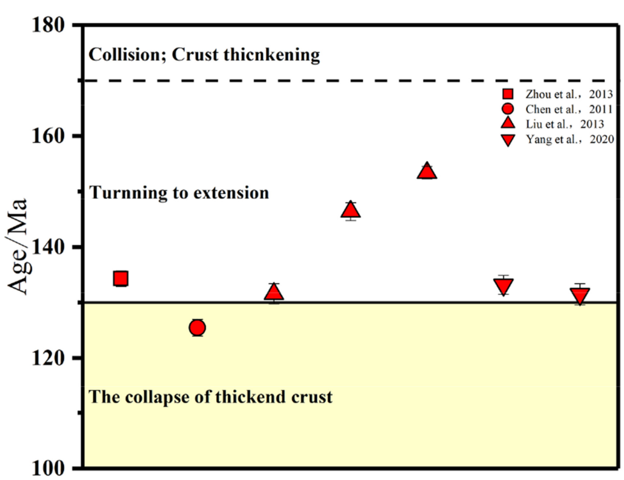

Fig. 5 Statistical map of isotopic age of the Xinxian pluton

that the Xinxian pluton was likely to have formed in the syn-collisional tectonic environment.

5.2 Fractional mechanism of iron isotopes in HFG

The value of δ^{56}Fe from all seven samples ranged from 0.19 to 0.36 ‰, which is consistent with the range of iron isotopes of granite (0.07–0.39 ‰) that has been reported in previous studies (Zhu et al. 2016). Some data with the content of $SiO_2 > 72$ wt.% were presented by Foden et al. (2015) and He et al. (2017). An obvious trend can be observed in Fig. 7a, which shows the HFG from the Xinxian pluton and that it is enriched in heavy iron isotopes with an increase in SiO_2. Compared with previous reports (Foden et al. 2015; He et al. 2017), the HFG from the Xinxian pluton is enriched with heavier iron isotopes, which may imply the existence of invisible mechanisms that have led to iron isotope fractionation, apart from fractional crystallization.

In the following section, the role of alteration and weathering, fluid exsolution, fractional crystallization, and partial melting is presented.

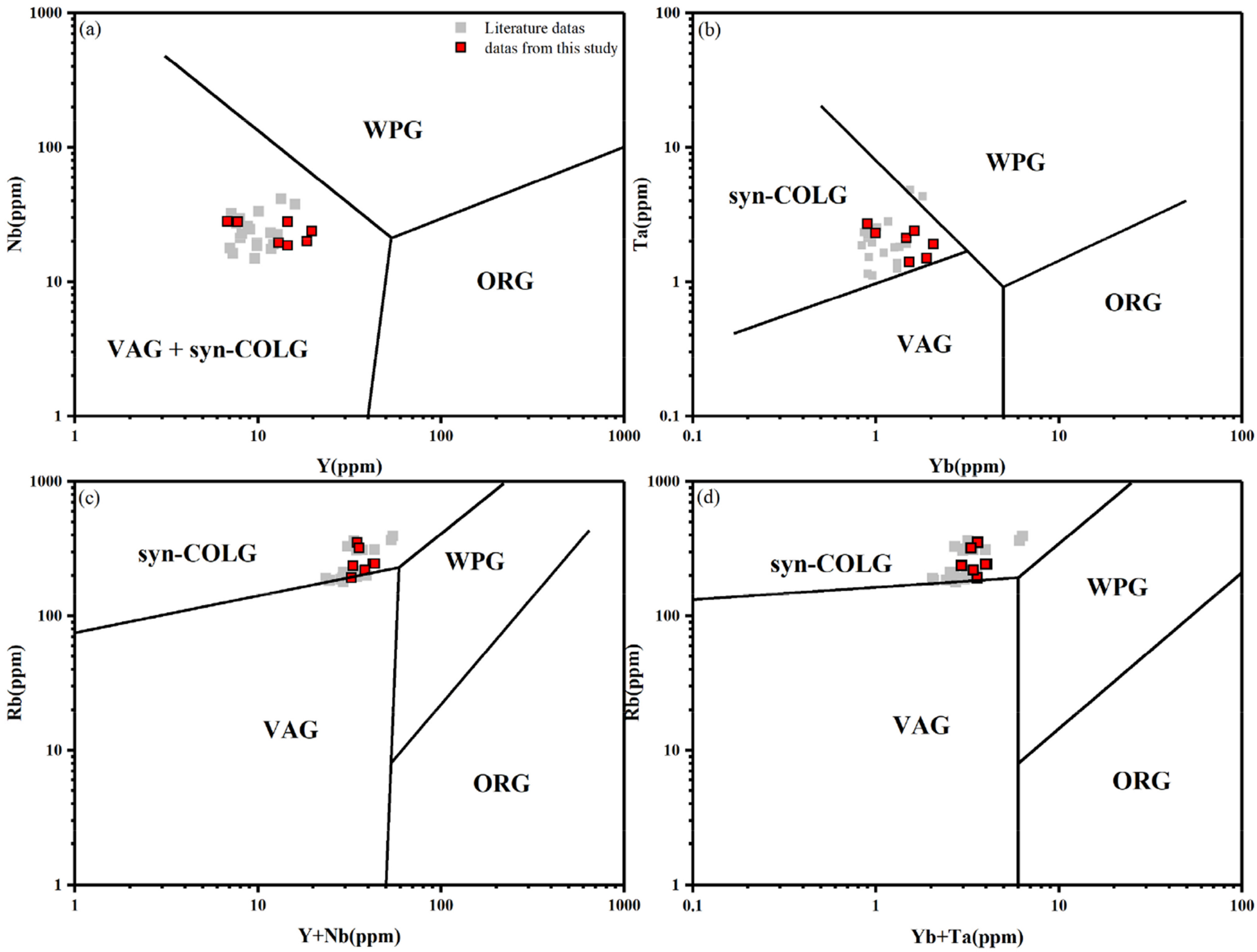

Fig. 6 Tectonic background discrimination diagram of the Xinxian pluton. WPG, intraplate granite. VAG, volcanic arc granite. ORG, oceanic ridge granite. and syn-COLG, syn-collisional granite

5.2.1 *Alteration and weathering*

Mineralogical observation (Fig. 3) showed that the feldspar and biotite in the samples were altered to different extents. Under the conditions of reductive weathering, the iron, decomposed by the weathering of primary minerals, can migrate in the form of Fe^{2+}, thus resulting in the enrichment of heavy iron isotopes (Liu et al. 2014; Poitrasson et al. 2008). However, under the conditions of oxidizing weathering, the free iron released by the weathering exists in the form of Fe^{3+} and leads to the presence of secondary minerals, without the loss of Fe or a change in iron isotopic composition (Liu et al. 2014). Notably, it is necessary to evaluate the influences of alteration and weathering on the Fe isotopic composition of the samples.

The LOI (loss of ignition) values of the samples were all lower than 1 wt.%. Moreover, there was no correlation between δ^{56}Fe and LOI, as shown in Fig. 7a. CIA (Al_2O_3/(Al_2O_3 + Na_2O + K_2O + CaO) in a mole fraction is the chemical index of alteration, which can be used to indicate the degree of weathering (Nesbitt and Young 1982). All samples displayed low CIA values (Fig. 7b) and no sign of weathering was observed. Ba and U are active elements, while Th and Nb are inactive elements. With the progress of alteration, Ba and U should be lost in the first place, thus resulting in a decrease in the Ba/Th value and an increase in Nb/U. However, both indexes failed to present the trend of alteration. Therefore, it was determined that alteration and weathering may not be the mechanisms that resulted in the fractionation of Fe isotopes in the HFG.

5.2.2 *Fluid exsolution*

It has been established that the fluid in intrusive rock can be discharged in the form of steam or brine (Audétat and Pettke 2003; Baker and Alletti 2012). Heimann et al. (2008) reported that fluid exsolution occurs in the late stage of the magmatic process, thus resulting in the enrichment

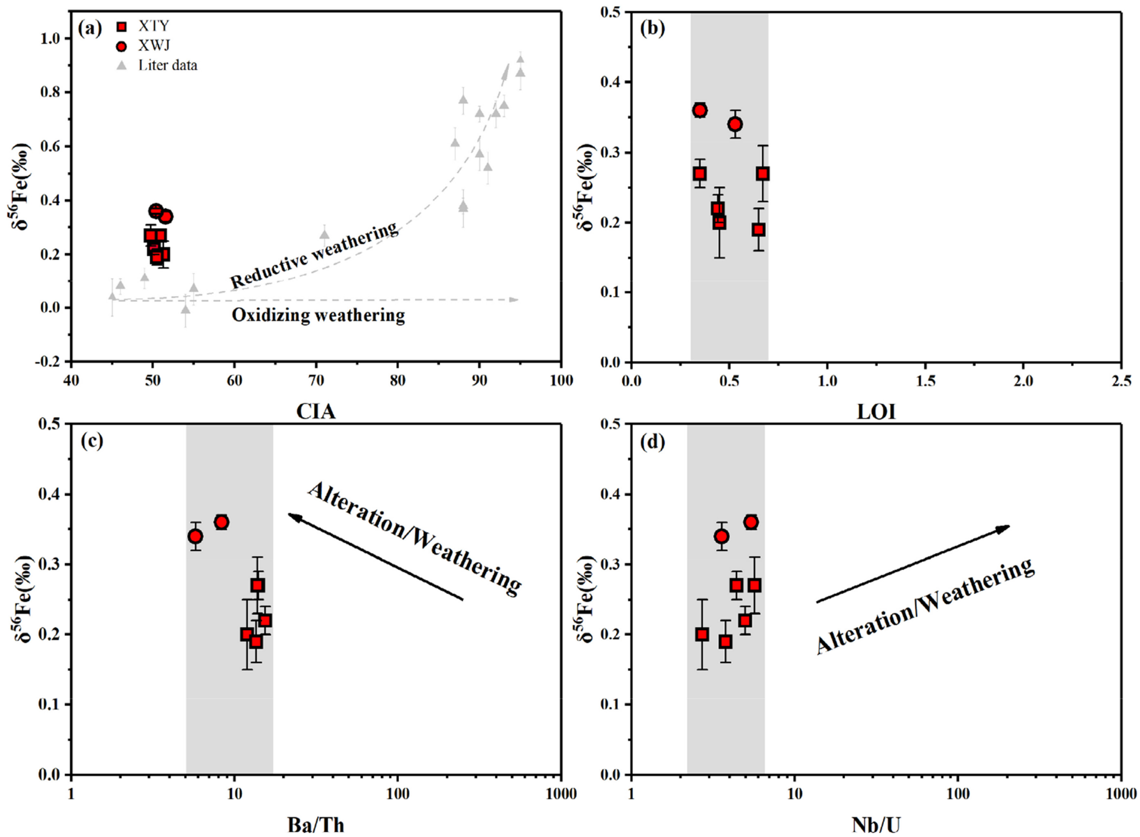

Fig. 7 δ^{56}Fe in HFG from Xinxian versus LOI (**a**), CIA (**b**), Ba/Th (**c**), Nb/U (**d**). The gray dotted line and literature data are from Liu et al. (2014). The gray dotted curve represents the reduced weathering trend, while the other dotted line represents the oxidizing weathering trend

of heavy iron isotopes in the melt by taking away the enriched light iron isotopes of Fe^{2+}.

The correlation between Zr/Hf, Nb/Ta, Rb/La, and δ^{56}Fe may provide constraints to the influences of fluid exsolution on iron isotope fractionation. The Zr/Hf ratios of igneous rock are generally less than 46 and higher than 26 (Bea et al. 2006), but significantly reduced after the exsolution of fluid because Zr is preferentially enriched in F-bearing fluid over Hf (Louvel et al. 2014). Previous studies (Ballouard et al. 2016) have argued that fluid exsolution occurred during the magmatic process, because the ratio of Nb/Ta is less than 5 (Du et al. 2019), as is also the case for Rb/La. The Th/U ratio used in this study is an index of fluid exsolution due to the higher mobility of U than Th in fluid (He et al. 2017).

The Zr/Hf ratios of two samples from XWJ were lower than 26, which may be explained by the effects of fluid exsolution, as shown in Fig. 8b. However, diagrams displaying another three parameters versus δ^{56}Fe show that the effects of fluid exsolution may be negligible. Both the XWJ granite and the XTY granite have Th/U values around the same levels as the mean lower continental crust (Th/U ~5.9, He et al. 2017) except for one sample (XTY-3-002, ~11.27). Recently, Du et al. (2019) argued that fluid exsolution may produce + 0.07 ‰ of δ^{56}Fe at most. Even if the high-level fluid exsolution occurred in the XTY or XWJ granite, the iron isotope fractionation of ~ 0.35 ‰ cannot be explained. Therefore, it was determined that another mechanism must be responsible for the enrichment of heavy iron isotopes in the Xinxian pluton.

5.2.3 Fractional crystallization and partial melting

The δ^{56}Fe of all the HFG samples increased with the increase in SiO_2 and $Fe^{3+}/\sum Fe$ and the decrease in Mg# and FeOt (Fig. 9), which suggested the influence of crystallization differentiation. The HFG trend can be modeled using the Rayleigh equation:

$$\delta^{56}Fe_{melt} = \delta^{56}Fe_{melt0} - \Delta^{56}Fe_{melt-crystal} \times \ln(f_{Fe}) \quad (2)$$

where f_{Fe} represents the Fe fraction in the remaining melt, and $\delta^{56}Fe_{melt0}$ refers to the value of δ^{56}Fe in the initial melt. XTY-4–002 was chosen on behalf of the composition of the initial melt to calculate the fractional factor of $\Delta^{56}Fe_{melt\text{-}crystal}$ due to its high FeOt content and low value of δ^{56}Fe. The results of the modeling are presented in Fig. 9b, which shows that the trend of fractional crystallization of

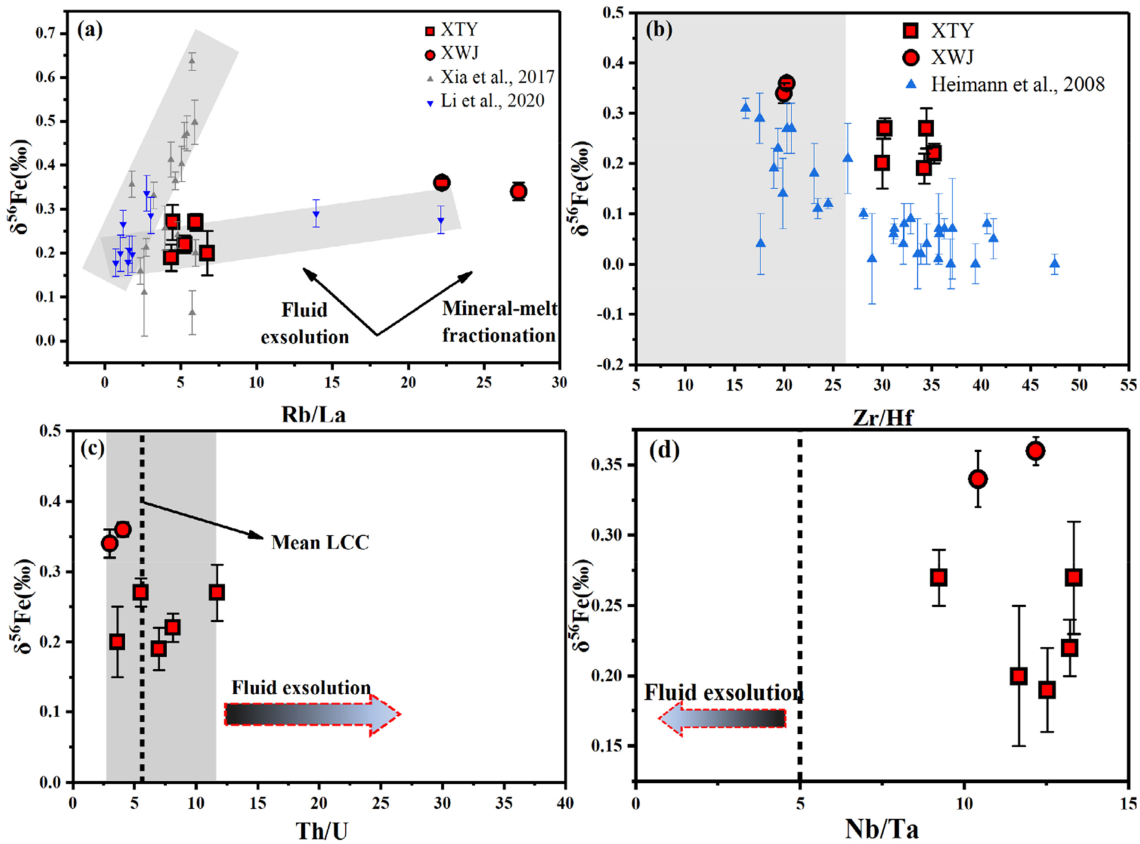

Fig. 8 δ^{56}Fe in HFG from Xinxian versus Rb/La (**a**), Zr/Hf (**b**), Th/U (**c**), Nb/Ta (**d**). The samples with Zr/Hf less than 26 in **b** tend to be affected by the dissolution of fluid. The gray field in **a** is the trend of δ^{56}Fe versus Rb/La ratios from Xia et al. (2017) and Li (2020), which is identical to the trend of HFG from the Xinxian pluton

HFG in the Xinxian pluton can be explained by $\Delta^{56}Fe_{melt\text{-}crystal}$ = ~ 0.15‰.

It has been reported in previous studies (Heimann et al. 2008; Telus et al. 2012; Sossi et al. 2012; Wu et al. 2017a, b) that olivine, pyroxene, hornblende, biotite, and Fe–Ti oxides are enriched with light iron isotopes, while feldspar and magnetite are enriched with heavy iron isotopes.

Olivine and pyroxene are barely crystallized from felsic magmas, which means that the crystallization of the two minerals may not drive evident Fe isotope fractionation. Owing to the enrichment of middle REEs in amphiboles, the separation of an amphibole may lead to the U-shaped REE pattern (Bachmann et al. 2005). In this study, an obvious Eu negative anomaly can be observed with a slightly right-inclining shape, excluding the effects on Fe isotope fractionation by the crystallization of the amphiboles.

The iron isotopic composition of feldspar is significantly heavier than those of other rock-forming minerals. Wu et al. (2017a, b) reported the δ^{56}Fe of migmatites that are formed by the feldspar accumulation in Dabie ranged from 0.424 ± 0.016 ‰ to 0.567 ± 0.016 ‰. Evidence from petrological observation showed that there was no sign of the accumulation of feldspar (Fig. 3). Furthermore, the accumulation of feldspar would produce a positive correlation between δ^{56}Fe value and Sr and Ba content as well as the Eu/Eu* ratio. Such correlation was not displayed in Fig. 10, so it was determined that the accumulation of feldspar may not account for the fractionation of iron isotopes in XWJ.

The crystallization of titanomagnetite, containing titanium spinel, might be the key factor affecting the Fe isotopic composition. Furthermore, the coefficient between titanomagnetite and the melt is ~ −0.1 ‰ (Schuessler et al. 2009). In conclusion, the crystallization of Fe–Ti oxide plays a significant role in the Fe isotopic composition of the residual melt, which has led to the enrichment of heavy Fe isotopes in the residual melt. The positive correlation between FeOt and TiO_2 in Fig. 11d shows the fractional crystallization of Fe–Ti oxide and the enrichment of heavy Fe isotopes in the residual melt.

Xu et al. (2017) suggested that FeOt/Al_2O_3 could be considered the enrichment index of feldspar for magmatic systems. As shown in Fig. 11a, the content of biotite in the samples was between 3 and 10%, and the Fe isotope

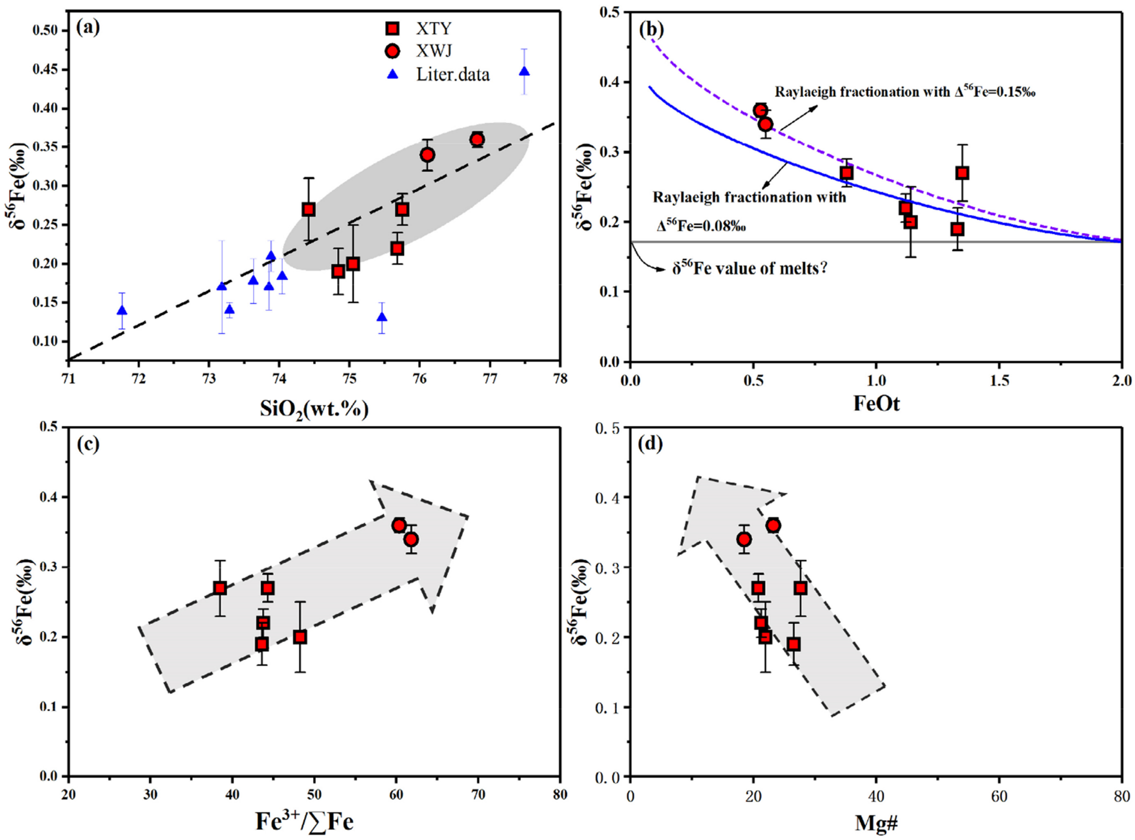

Fig. 9 δ^{56}Fe in HFG from Xinxian versus SiO_2 (**a**), FeOt (**b**), $Fe^{3+}/\sum Fe$ (**c**), Mg# (**d**). The literature data in **a** are from He et al. (2017) and Foden et al. (2015). The two curves in **b** are modeled by Rayleigh equation

composition was significantly heavier than the estimated curve. We hold the view that this is probably due to the influence of the melt composition.

The magma evolves towards acidity with an increase in SiO_2, while the alkali elements (Na and K) in feldspar tend to be enriched. The enrichment of these alkali metals, resulting in Fe^{3+} in the melt, becomes more stable in the tetra-coordination (Métrich et al. 2006; Guili et al. 2012), which leads to the accumulation of heavy iron isotopes. The positive correlation between δ^{56}Fe and (Na + K)/(Ca + Mg) (in mole fraction), as presented in Fig. 11b, shows that the variable δ^{56}Fe from the HFG can be attributed to the magma composition, given that the HFG fall within the global HSG trend, thus leading to changes in $\Delta^{56}Fe_{\text{melt-crystal}}$.

Notably, once the composition of the melt changes, the composition of the mineral will change accordingly. Wu et al. (2017a, b) argued that the change in mineral composition would significantly affect the fractionation of iron isotopes between minerals. Wu et al. (2017a, b) created the equation between $\Delta^{56}Fe_{\text{Plagioclase-Biotite}}$, $\Delta^{56}Fe_{\text{Alkali-feldspar-Biotite}}$, $\Delta^{56}Fe_{\text{Plagioclase-Magnetite}}$, $\Delta^{56}Fe_{\text{Plagioclase-Magnetite}}$, $\Delta^{56}Fe_{\text{Alkali-feldspar-Magnetite}}$, and the content of Ab and Or:

$$\Delta^{56}Fe_{\text{Plagioclase-Biotite}} = 0.015 \times Ab - 0.48 \quad (3)$$

$$\Delta^{56}Fe_{\text{Alkali-feldspar-Biotite}} = 0.026 \times Or - 0.48 \quad (4)$$

$$\Delta^{56}Fe_{\text{Plagioclase-Magnetite}} = 0.022 \times Ab - 1.15 \quad (5)$$

$$\Delta^{56}Fe_{\text{Alkali-feldspar-Magnetite}} = 0.026 \times Or - 1.46 \quad (6)$$

The Δ^{56}Fe result according to this calculation is shown in Table 4. The calculated results of Δ^{56}Fe between feldspar and biotite/magnetite demonstrate that the change in the mineral composition may not be responsible for the iron isotopic composition of HFG, because the measured value of δ^{56}Fe is significantly heavier than the calculated result of Δ^{56}Fe.

The effects of partial melting on iron isotopes are complex and involve oxygen fugacity and the degree of melting (Zhu et al. 2016). Xu et al. (2017) discovered that partial melting can trigger the fractionation of iron isotopes, averaging 0.093 ± 0.056‰ between leucosome (product of partial melting) and melanosome (residual of partial melting) in migmatite under the conditions of P = ca. 5.0 kbar, T = 705–744 °C. Previous studies have shown that the source rocks of the Xinxian HFG were Neoproterozoic TTG magmatic rocks from the north margin of the Yangtze block and were derived from the middle

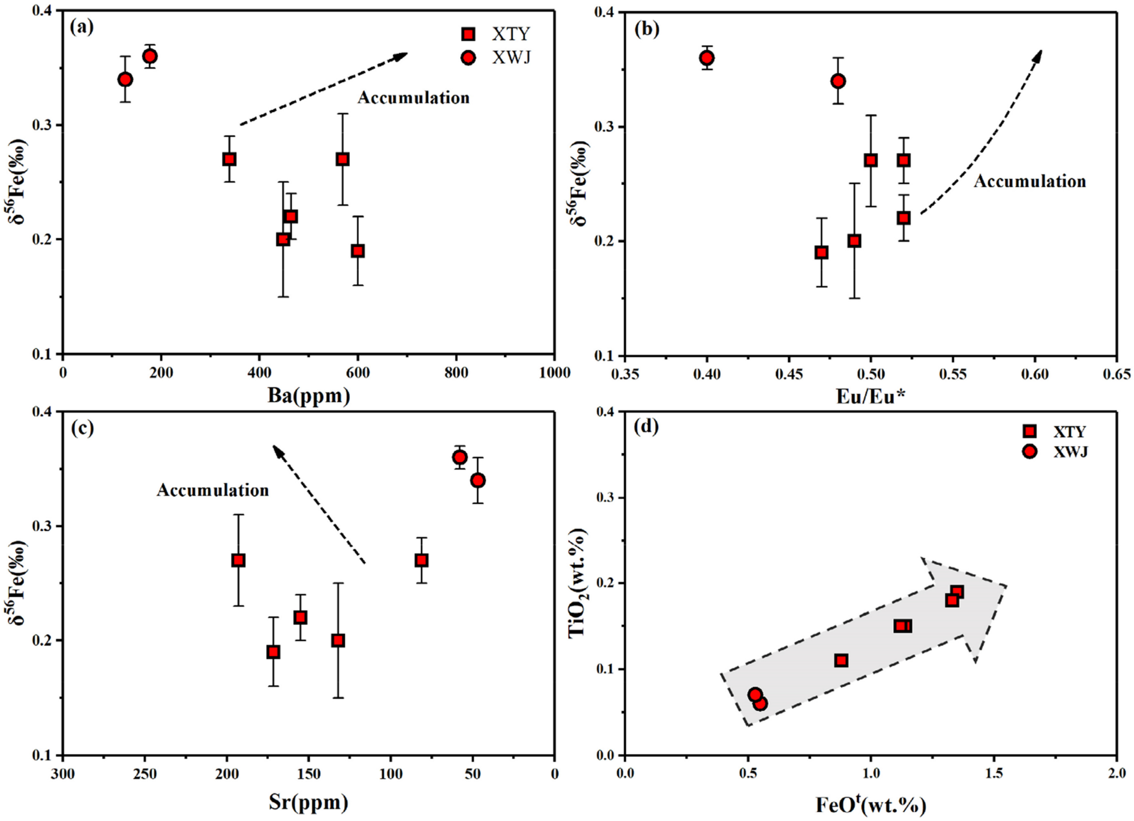

Fig. 10 δ^{56}Fe in HFG from Xinxian versus Ba (**a**), Eu/Eu* (**b**), Sr (**c**); diagram of TiO_2 vs. FeOt (**d**)

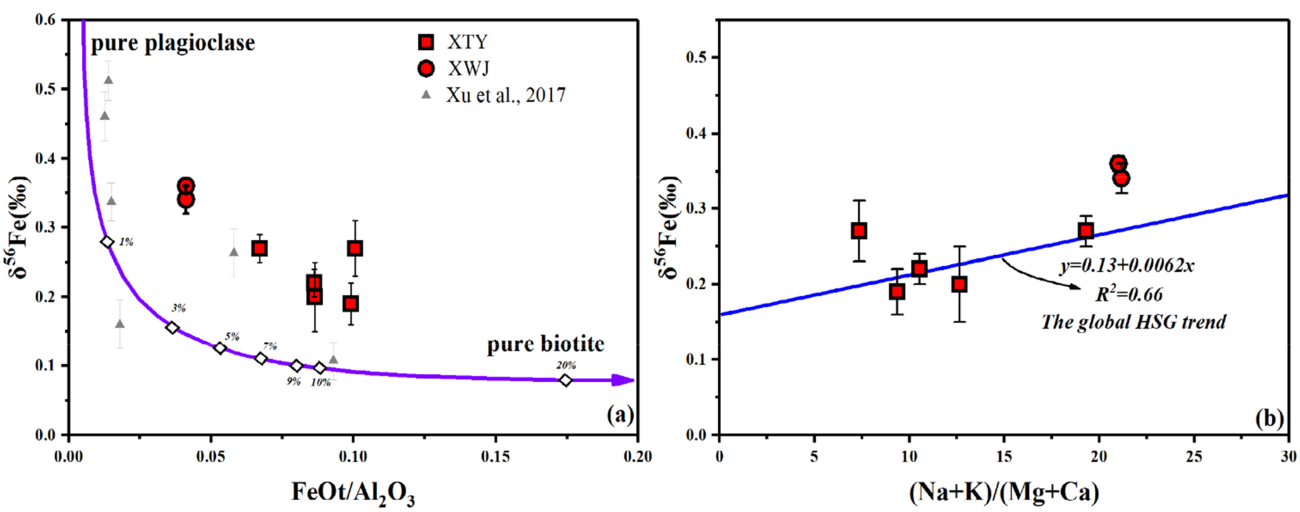

Fig. 11 δ^{56}Fe in HFG from Xinxian versus FeOt/Al_2O_3 (**a**), (Na + K/Ca + Mg) (**b**). The curve in **a** is from Xu et al. (2017), and the percentage numbers denote the fraction of biotite. The global HSG in **b** is from He et al. (2017)

and lower crust with a low temperature (< 800 °C) and a depressurized environment (Chen et al. 2013a; Zhao et al. 2013; Yang et al. 2020). Moreover, Li (2020) reported the iron isotopic composition of Early and late Neoarchean TTG type magmatic rocks, and the results illustrated that the values of ^{56}Fe in TTG magmatic rocks with different ages and regions are similar, ranging from 0.075 ‰ to 0.201 ‰, with an average of 0.142 ± 0.07 ‰. In that case, partial melting may also lead to iron isotopic fractionation before the fractional crystallization. However, it is difficult to estimate the influences of partial melting using our current evidence.

Table 4 Calculation results of $\Delta^{56}Fe$ between feldspar and dark minerals

	XTY-1–001	XTY-2–001	XTY-3–002	XTY-3–003	XTY-4–002	XWJ-001	XWJ-003	Avergae
$\Delta^{56}Fe_{Plg\text{-}Bi}$	0.046	0.003	0.013	0.041	0.016	0.048	0.062	0.033
$\Delta^{56}Fe_{Afs\text{-}Bi}$	−0.616	−0.601	−0.63	−0.667	−0.608	−0.647	−0.661	−0.633
$\Delta^{56}Fe_{Plg\text{-}Mgn}$	−0.378	−0.441	−0.426	−0.385	−0.421	−0.374	−0.353	−0.397
$\Delta^{56}Fe_{Afs\text{-}Mgn}$	−0.726	−0.711	−0.74	−0.777	−0.718	−0.757	−0.771	−0.743

6 Conclusions

(1) Major elements and mineralogical observations showed that the early Cretaceous granite in the Xinxian pluton belongs to the highly fractionated I-type granite.
(2) Further investigation demonstrated that the effect of fluid exsolution, along with alteration and weathering, on the Fe isotopes in HFG is negligible.
(3) The results modeled using the Rayleigh equation showed that fractional crystallization may produce $\Delta^{56}Fe_{melt\text{-}crystal}$ = 0.08 ‰ ∼ 0.15 ‰. The controlling factor that contributes to the Fe isotopic composition of our sample might be the fractional crystallization of Fe-Ti oxides.
(4) The change in melt composition may also lead to the enrichment of heavy Fe isotopes in the residual melt, while the role of partial melting is consistent with the current observations.

Acknowledgements We appreciate professor Huang for his help in the measurement of iron isotopes and Miss Tan for the Language editing advice. We also thank our team members who contributed to this study

Funding National Natural Science Foundation of China, Grant/Award number: 41972169. The priority academic program development of Jiangsu Higher Education on Institutions (2018–2021).

Declarations

Conflict of interest The authors declare that they have no conflict of interest.

References

Audétat A, Pettke T (2003) The magmatic-hydrothermal evolution of two Barren granites: a melt and fluid inclusion study of the Rito del Medio and Canada Pinabe Plutons in Northern New Mexico (USA). Geochim Cosmochim Acta 67(1):97–121. https://doi.org/10.1016/S0016-7037(02)01049-9

Bachmann O, Dungan MA, Bussy F (2005) Insights into shallow magmatic processes in large silicic magma bodies: the trace element record in the Fish Canyon magma body. Colorado Contrib Mineral Petrol 149(3):338–349. https://doi.org/10.1007/s00410-005-0653-z

Baker DR, Alletti M (2012) Fluid saturation and volatile partitioning between melts and hydrous fluids in crustal magmatic systems: the contribution of experimental measurements and solubility models. Earth-Sci Rev 114(3–4):298–324. https://doi.org/10.1016/j.earscirev.2012.06.005

Ballouard C, Poujol M, Boulvais P et al (2016) Nb-Ta fractionation in peraluminous granites: a marker of the magmatic-hydrothermal transition. Geology 44(3):231–234. https://doi.org/10.1130/G37475.1

Bea AF, Montero P, Ortega M (2006) A LA-ICP-MS evaluation of Zr reservoirs in common crustal rocks: implications for Zr and Hf geochemistry, and zircon-forming processes. Can Mineral 44(3):693–714. https://doi.org/10.2113/gscanmin.44.3.693

Chappel BW, White AJR (1992) I- and S-type Granites in the Lachlan fold belt. Earth Environ Sci Trans R Soc Edinb 83(1–2):1–26. https://doi.org/10.1130/SPE272-p1

Chen W, Xu ZW, Li HC et al (2013a) Petrogenesis and origin of the Xinxian Granitic Batholith in Henan Province and its implication for the Tectonic evolution of the Western Dabie Area. Acta Geol Sin 87(10):1510–1524 (**in Chinese with English abstract**)

Chen W, Xu ZW, Qiu WH et al (2015) Petrogenesis of the Yaochong granite and Mo deposit, western Dabie Orogen, Eastern-central China: Constraints from zircon U-Pb and molybdenite Re–Os ages, whole-rock geochemistry and Sr–Nd–Pb–Hf isotopes. J Asian Earth Sci 103:198–211. https://doi.org/10.1016/j.jseaes.2015.01.010

Chen YH, Niu YL, Duan M et al (2021) Fractional crystallization causes the iron isotopes contrast between mid-ocean ridge basalts and abyssal peridotites. Commun Earth Environ 2(1):1–9. https://doi.org/10.1038/s43247-021-00135-5

Chen W, Xu ZW, Lu XC et al (2013b) Petrogenesis of the Bao'anzhai granite and associated Mo mineralization, western Dabie Orogen, East-central China: Constraints from zircon U–Pb and molybdenite Re–Os dating, whole-rock geochemistry, and Sr–Nd–Pb–Hf Isotopes. Int Geol Revi 55(10):1220–1238. https://doi.org/10.1080/00206814.2013.772322

Cin-Ty AL, Douglas MM (2015) High silica granites: terminal porosity and crystal settling in shallow magma chambers. Earth Planet Sci Lett 409:23–31. https://doi.org/10.1016/j.epsl.2014.10.040

Collinet M, Charlier B, Namur O et al (2017) crystallization history of enriched shergottites from Feand Mg isotopes fractionation in Olivine Megacrysts. Geochim Cosmochim Acta 207(15):277–297. https://doi.org/10.1016/j.gca.2017.03.029

Deng CL, Hu CQ, Li M et al (2021) Iron isotope composition of Adakitic Rocks: The Shangcheng Pluton. Western Dabie Orogen, Central China. Minerals 11(12):1356–1370. https://doi.org/10.3390/min11121356

Deng JH, He YS, Zartman RE et al (2022) Large iron isotope fractionation during mantle wedge serpentinization: Implications for iron isotopes of arc magmas. Earth Planet Sci Lett 583:1–8. https://doi.org/10.1016/j.epsl.2022.117423

Du DH, Wang XL, Yang T et al (2017) Origin of heavy fe isotopes compositions in high-silica igneous rocks: a rhyolite perspective.

Geochim Cosmochim Acta 218:58–72. https://doi.org/10.1016/j.gca.2017.09.014

Du DH, Li WQ, Wang XL et al (2019) Fe isotopic fractionation during the magmatic-hydrothermal stage of granitic magmatism. Lithos 350–351:1–13. https://doi.org/10.1016/j.lithos.2019.105265

Foden J, Sossi PA, Wawryk CM (2015) Fe isotopes and the contrasting petrogenesis of A-, I-and S-type granite. Lithos 212–215:32–44. https://doi.org/10.1016/j.lithos.2014.10.015

Guili G, Alonso-Mori R, Cicconi MR et al (2012) Effect of alkalis on the Fe oxidation state and local environment in peralkaline rhyolitic glasses. Am Miner 97:468–457. https://doi.org/10.2138/am.2012.3888

He YS, Li SG, Hoefs J et al (2011) Post-collisional Granitoids from the Dabie Orogen: new evidence for partial melting of a thickened continental crust. Geochim Cosmochim Acta 75(13):3815–3838. https://doi.org/10.1016/j.gca.2011.04.011

He YS, Li SG, Hoefs J et al (2013) Sr-Nd-Pb isotopic compositions of early cretaceous Granitoids from the Dabie Orogen: constraints on the recycled lower continental crust. Lithos 156–159:204–217. https://doi.org/10.1016/j.lithos.2012.10.011

He YS, Wu HJ, Ke S et al (2017) Iron isotopic compositions of adakitic and non-adakitic graniti-c magmas: magma compositional control and sub-tle residual garnet effect. Geochim Cosmochim Acta 203:89–103. https://doi.org/10.1016/j.gca.2017.01.005

Heimann A, Beard LB, Johnson CM (2008) The role of volatile exsolution and sub-solidus fluid/r-ock interactions in producing high $^{56}Fe/^{54}Fe$ ratios in siliceous igneous rocks. Geochim Cosmochim Acta 72(17):4379–4396. https://doi.org/10.1016/j.gca.2008.06.009

Huang F, Zhang Z, Lundstrom CC et al (2011) Ir-on and magnesium isotopic compositions of peridotite xenoliths from Eastern China. Geochim Cosmochim Acta 75(12):3318–3334. https://doi.org/10.1016/j.gca.2011.03.036

Huang DF, Lu XX, Luo ZH et al (2018) Zircon SHRIMP U-Pb Age, Geochemical Characteristics and Geological Implications of Shangcheng Pluton in the Northern Margin of Dabie Mountain. Earth Sci 44(11):3829–3844. https://doi.org/10.3799/dqkx.2018.558 (in Chinese with English abstract)

Li RY (2020) Evolution of the Archean continental crust and link to the great oxidation event traced by Mg, Fe isotopes: [Dissertation]. China University of Geoscience Beijing, Beijing, pp 1–139 (in Chinese with English abstract)

Li SG, Jagoutz E, Lo CH et al (1999) Sm/Nd, Rb/Sr, and $^{40}Ar/^{39}Ar$ Isotopic systematics of the Ult-rahigh-pressure metamorphic rocks in the Dabie- Sulu Orogenic Belt, Central China: a retrospective view. Int Geol Rev 41(12):1114–1124. https://doi.org/10.1080/00206819909465195

Liang WL, Huang J, Zhang GB et al (2022) Iron isotopic fractionation during eclogite anatexis and adakitic melt evolution: insights into garnet effect on Fe isotopic variations in high-silica igneous rocks. Contrib Miner Petrol 177:33–50. https://doi.org/10.1007/s00410-022-01898-6

Liu XC, Jahn BM, Liu DY et al (2004) SHRIMP U-Pb Zircon dating of a metagabbro and eclogites from western Dabieshan (Hong'an Block), China, and its tectonic implications. Tectonophysics 394(3):171–192. https://doi.org/10.1016/j.tecto.2004.08.004

Liu SA, Teng FZ, Li SG et al (2014) Copper and iron isotopes fractionation during weathering and Pedogenesis: insights from Saprolite profiles. Geochim Cosmochim Acta 146:59–75. https://doi.org/10.1016/j.gca.2014.09.040

Loiselle MC, Wones DR (1979) Characteristics and origin of Anorogenic Granites. Geol Soci Am 11:468–468. https://www.researchgate.net/publication/313197089_Characteristics_of_an_orogenic_granite

Louvel M, Sanchez-Valle C, Malfait WJ et al (2014) Constraints on the mobilization of Zr in magmatic-hydrothermal processes in subduction zones from in situ fluid-melt partitioning experiments. Am Miner 99(8–9):1616–1625. https://doi.org/10.2138/am.2014.4799

McDonough WF, Sun SS (1995) The composition of the Earth. Chem Geol 120(3–4):223–253. https://doi.org/10.1016/0009-2541(94)00140-4

Meng F (2013). Study on rock-forming and ore-forming of the Lingshan Pluton in the Northern margin of Dabie mountains: [Dissertation]. China University of Geosciences (Beijing), Beijing.112–120 (in Chinese with English abstract)

Métrich N, Susini J, Foy E et al (2006) Redox state of iron in Peralkaline Rhyolitic Glass/Melt: X-ray absorption micro-spectroscopy experiments at high temperature. Chem Geol 231(4):350–363. https://doi.org/10.1016/j.chemgeo.2006.02.001

Nesbitt HW, Young GM (1982) Early proterozoic climates and plate motions inferred from major element chemistry of lutites. Nature 299:715–717

Niu PP, Jiang SY (2020) Petrogenesis of the Late Mesozoic Qijinfeng granite complex in the Tongbai Orogen: Geochronological, geochemical and Sr-Nd-Pb-Hf isotopes evidence. Lithos 365–367:1–17. https://doi.org/10.1016/j.lithos.2019.105290

Poitrasson F, Freydier R (2005) Heavy iron isotopes composition of granites determined by high resolution MC-ICP-MS. Chem Geol 222(1–2):132–147. https://doi.org/10.1016/j.chemgeo.2005.07.005

Poitrasson F, Viers J, Martin F et al (2008) Limited iron isotopes variations in recent lateritic soils from Nsimi, Cameroon: implications for the global Fe geochemical cycle. Chem Geol 253(1–3):54–63. https://doi.org/10.1016/j.chemgeo.2008.04.011

Schuessler JA, Schoenberg R, Sigmarsson O (2009) Iron and Lithium isotopes systematics of the Hekla Volcano, Iceland: evidence for Fe isotopes fractionation during magma differentiation. Chem Geol 258(1–2):78–91. https://doi.org/10.1016/j.chemgeo.2008.06.021

Sossi PA, Foden JD, Halverson GP (2012) Redox-controlled Iron Isotopes fractionation during magmatic differentiation: an example from the red hill intrusion, S. Tasmania Contrib Mineral Petrol 164(5):757–772. https://doi.org/10.1007/s00410-012-0769-x

Sun SS, McDonough WF (1989) Chemical and isotopic systematics of oceanic basalts: implications for mantle composition and processes. Geol Soc Lond Spec Publ 42(1):313–345. https://doi.org/10.1144/gsl.sp.1989.042.01.19

Suo ST, Zhong ZQ, Zhou HW et al (2012) Two fresh types of eclogites in the Dabie-Sulu UHP Metamorphic Belt, China: implications for the deep subduction and earliest stages of exhumation of the continental crust. J Earth Sci 23(6):775–785. https://doi.org/10.1007/s12583-012-0295-9

Telus M, Dauphas N, Moynier F et al (2012) Iron, zinc, magnesium and uranium isotopic fractionation during continental crust differentiation: the tale from migmatites, granitoids, and pegmatites. Geochim Cosmochim Acta 97:247–265. https://doi.org/10.1016/j.gca.2012.08.024

Teng FZ, Dauphas N, Helz RT et al (2011) Diffusion-driven magnesium and iron isotopes fractionation in Hawaiian Olivine. Earth Planet Sci Lett 308(3):317–324. https://doi.org/10.1016/j.epsl.2011.06.003

Weyer S, Ionov DA (2007) Partial melting and melt percolation in the mantle: the message from Fe isotopes. Earth Planet Sci Lett 259(1–2):119–133. https://doi.org/10.1016/j.epsl.2007.04.033

Whalen JB, Currie KL, Chappell BW (1987) A-types granites: geochemical characteristics, discrimination and petrogenesis. Contrib Mineral Petrol 95(4):369～383. https://doi.org/10.1007/BF00402202

Williams HM, Peslier AH, Mccammon C et al (2005) Systematic iron isotopes variations in mantle rocks and minerals: the effects of partial melting and oxygen fugacity. Earth Planet Sci Lett 235(1–2):435–452. https://doi.org/10.1016/j.epsl.2005.04.020

Wu HJ, He YS, Bao L et al (2017a) Mineral composition control on inter-mineral iron isotopic fractionation in granitoids. Geochim Cosmochim Acta 198:208–217. https://doi.org/10.1016/j.gca.2016.11.008

Wu FY, Liu XC, Ji WQ et al (2017b) Highly fractionated granites: recognition and research. Scie Sinica (terrae) 47(7):745–765. https://doi.org/10.1360/N072016-00139

Xia Y, Li SQ, Huang F (2017) Iron and zinc isotope fractionation during magmatism in the continental crust: evidence from bimodal volcanic rocks from Hailar Basin, NE China. Geochim Cosmochim Acta 213:35–46. https://doi.org/10.1016/j.gca.2017.06.018

Xu HJ, Ma CQ, Ye K (2007) Early cretaceous granitoids and their implications for the collapse of the Dabie Orogen, Eastern China: SHRIMP Zirc-on U-Pb Dating and Geochemistry. Chem Geol 240(3–4):238–259. https://doi.org/10.1016/j.chemgeo.2007.02.018

Xu HJ, Ma CQ, Zhang JF et al (2012) Early cretaceous low-Mg adakitic Granites from the Dabie Orogen, Eastern China: petrogenesis and implications for destruction of the over-thickened lower continental crust. Gondwana Res 23(1):190–207. https://doi.org/10.1016/j.gr.2011.12.009

Xu LJ, He Y, Wang SJ et al (2017) Iron isotope fractionation during crustal Anatexis: constraint-s from Migmatites from the Dabie Orogen, Central China. Lithos 284:171–179. https://doi.org/10.1016/j.lithos.2017.04.005

Yang CY, He J, Yang YZ et al (2020) Geochemical Characteristics and Petrogenesis of Monzogranites from the Xinxian Batholith, Dabie Orogenic Belt. Geological Journal of University, 26(2):132–146. https://doi.org/10.16108/j.issn1006-7493.2019031 (in Chinese with English abstract)

Yang F (2019) Highly fractionated granite: mineral, geochemical features and their implications: [Dissertation]. China University of Geoscience Beijing, Beijing, pp 1–93 (in Chinese with English abstract)

Zhao ZF, Zheng YF, Wei CS et al (2007) Post-collisional granitoids from the Dabie Orogen in China: Zircon U-Pb Age, element and O isotopes evidence for recycling of subducted continental crust. Lithos 93(3–4):248–272. https://doi.org/10.1016/j.lithos.2006.03.067

Zhao ZX, Yang XN, Xu ZW et al. (2013) Research on thermometers and barometers of early Cretaceous Granite in Xinxian County, Henan Province, China. J Nanjing Univ 49(06):747–761. https://doi.org/10.13232/j.cnki.jnju.2013.06.013

Zheng YF (2008) Research progress on UHP metamorphism and continental collision: a case study of Dabie Sulu Orogenic Belt. Chin Sci Bull 53(18):2129–2152 (**in Chinese with English abstract**)

Zheng YF, Wang ZR, Li SG (2003a) Oxygen isotopes equilibrium ultrahigh-pressure metamorphic minerals and its constraints on Sm-Nd and Rb-Sr Chronometers. Geol Soc Lond Spec Publ 220(1):93–117. https://doi.org/10.1144/GSL.SP.2003.220.01.06

Zheng YF, Fu B, Gong B et al (2003b) Stable isotope geochemistry of ultrahigh pressure metamorphic rocks from the Dabie-Sulu orogen in China: implications for geodynamics and fluid regime. Earth Sci Rev 62(1–2):105–161. https://doi.org/10.1016/S0012-8252(02)00133-2

Zhou HS, Liu MH, Yan YT (2013) Zircon U-Pb age of Xinxian Pluton in Dabie Orogenic belt and its geological implications. J Xinyang Normal Univ Nat Sci Edition 26(01):94–98. https://doi.org/10.3969/j.issn.1003-0972.2013.01.022

Zhu XK, Sun J, Wang Y (2016) Fe isotopes geochemistry of magmatic system. J Earth Sci Environ 38(1):1–10. https://doi.org/10.3969/j.issn.1672-6561.2016.01.001(inChinesewithEnglishabstract)

Zhu J, Wu CX, Peng SG et al (2019) U-Pb Zircon Age, geochemistry and isotopic characteristics of the Tanchong and Chenchong Granites in the Western Dabie Orogen, China: Constraints on Petro-genesis and Timing of Lower Crustal Delamination. Acta Geol Sin 93(7):1671–1686. https://doi.org/10.19762/j.cnki.dizhixuebao.2019054 (in Chinese with English abstract)